Seasonal variations of O2 atmospheric and OH(6?2) airglowand temperature at mid-latitudes from SATI observations

M. J. López-González, Elizandro Rodriguez, R. H. Wiens, G. G. Shepherd, S. Sargoytchev, S. Brown, M. G. Shepherd, V. M. Aushev, J. J. López-Moreno, R. Rodrigo, et al.

Annales Geophysicae (2004) 22: 819–828
SRef-ID: 1432-0576/ag/2004-22-819

Annales Geophysicae

Seasonal variations of O_2 atmospheric and OH(6–2) airglow and temperature at mid-latitudes from SATI observations

M. J. López-González[1], E. Rodríguez[1], R. H. Wiens[2], G. G. Shepherd[3], S. Sargoytchev[3], S. Brown[3], M. G. Shepherd[3], V. M. Aushev[4], J. J López-Moreno[1], R. Rodrigo[1], and Y.-M. Cho[3]

[1]Instituto de Astrofísica de Andalucía, CSIC, P.O. Box 3004, E-18080 Granada, Spain
[2]Department of Physics, University of Asmara, Eritrea
[3]Centre for Research in Earth and Space Science, York University, 4700 Keele St., Toronto, Ontario M3J 1P3, Canada
[4]Institute of Ionosphere, Ministry of Education and Science, Almaty, 480020, Kazakhstan

Received: 26 February 2003 – Revised: 17 September 2003 – Accepted: 12 November 2003 – Published: 19 March 2004

Abstract. More than 3 years of airglow observations with a Spectral Airglow Temperature Imager (SATI) installed at the Sierra Nevada Observatory (37.06° N, 3.38° W) at 2900 m height have been analyzed. Values of the column emission rate and vertically averaged temperature of the O_2 atmospheric (0–1) band and of the OH Meinel (6–2) band from 1998 to 2002 have been presented. From these observations a clear seasonal variation of both emission rates and rotational temperatures is inferred at this latitude. It is found that the annual variation of the temperatures is larger than the semi-annual variation, while for the emission rates the amplitudes are comparable.

Key words. Atmospheric composition and structure (airglow and aurora; pressure density and temperature; instruments and techniques)

1 Introduction

Airglow emissions give important information on the dynamics and chemistry of the upper atmosphere. After the discovery of the vibration-rotation of the OH Meinel system in the night airglow by Meinel (1950a), a great number of works have been devoted to the observation of the temporal variations of the emission rates and rotational temperatures of the OH Meinel bands (e.g. Shefov, 1969, 1971a; Takahashi et al., 1977; Mulligan et al., 1995). These measurements have shown a great variability for the different OH Meinel bands. On the other hand, measurements of volume emission profile have shown the peak of the maximum emission rate at around 87 km (Baker and Stair, 1988). Rotational temperatures from the OH Meinel bands have been used as indicators of atmospheric temperature at 87 km height.

Since the O_2(0–1) atmospheric band at 8645 A is free from absorption, it can be observed by ground-based optical techniques. Meinel (1950b) observed it using a spectrograph and obtained the rotational temperature T_{O_2}. The nocturnal emission variation of this band has been observed at different latitudes by different investigators (e.g. Misawa and Takeuchi, 1977, 1982; Takahashi et al., 1986; Burrage et al., 1994). Rocket and satellite measurements have shown that the peak of maximum emission rate of the O_2 atmospheric emission is placed at about 95 km (e.g. Witt et al., 1979, 1984; Greer et al., 1986). So, rotational temperatures from the O_2(0–1) atmospheric band are good indicators of the atmospheric temperature at around 95 km height.

The Spectral Airglow Temperature Imager (SATI) is an instrument able to measure the column emission rate and vertically averaged rotational temperature of both the O_2 atmospheric (0–1) band, and the OH Meinel (6–2) band, using the technique of interference filter spectral imaging with a cooled-CCD detector. The technique was first developed by the Mesopause Oxygen Rotational Temperature Imager (MORTI) instrument (Wiens et al., 1991). The new adaptation on SATI is described by Wiens et al. (1997).

In this paper we introduce briefly the SATI instrument and the method of SATI image reduction. Then we show initial results from the SATI airglow observations at 37.06° N latitude after more than three years of data. Seasonal variations of the temperature and airglow emission rates of the O_2 atmospheric (0–1) band and the OH Meinel (6–2) band are presented and compared with previous results.

2 Instrument

SATI is a spatial and spectral imaging Fabry-Perot spectrometer in which the etalon is a narrow band interference filter and the detector is a CCD camera. SATI represents an improved adaptation of the MORTI instrument. The SATI instrumental concept and optical configuration is that of MORTI. Its field of view is an annulus of 30° average radius and 7.1° angular width centered on the zenith. Thus, an annulus of average radius of 55 km and 16 km width at 95 km of altitude (or an average radius of 49 km and 14 km width at

Correspondence to: M. J. López-González
(mariajose@iaa.es)

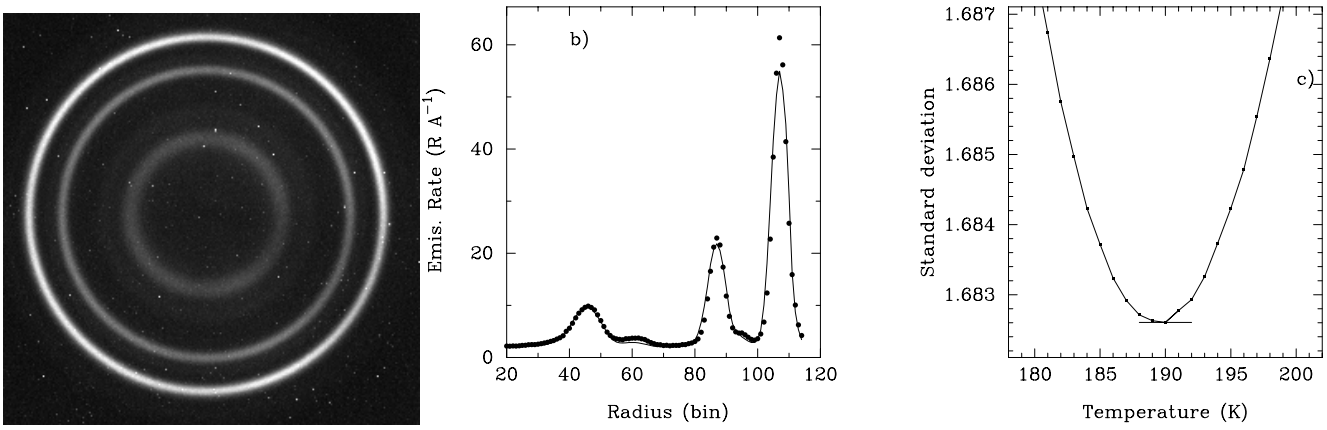

Fig. 1. **(a)** Typical OH SATI image. **(b)** Calculated (solid line) and observed (points) radial signal distribution for above OH image. Parameters are: A=920 R, B=2.0 R A^{-1}, T=190° K . **(c)** Standard deviation of the fit versus temperature.

85 km) is observed in the sky. SATI uses two interference filters, one centred at 867.689 nm (in the spectral region of the O_2 atmospheric (0–1) band) and the second one centred at 836.813 nm (in the spectral region of the OH Meinel (6–2) band).

The images are disks where the azimuth dimension corresponds to the azimuth of the ring of the sky observed, while the radial distribution of the images contains the spectral distribution, from which the rotational temperature is inferred.

The images obtained from SATI can be analyzed as a whole, obtaining an average of the rotational temperature and emission rate of the airglow band from the whole sky ring; this allows for a good monitoring of the behaviour of the rotational temperature and emission rate for long periods of time, or by dividing the images into different sectors thus, obtaining information of rotational temperatures and emission rates of each sector of the sky ring, from which the horizontal velocity of a disturbance can be determined (Zhang et al., 1993).

2.1 O_2(0–1) atmospheric system

The PP and PQ branches of the spectrum of the O_2 atmospheric (0–1) band appear as pairs of lines of 0.13 nm in separation, and these pairs are separated from each other by 0.32 nm. These line pairs, in convolution with the 0.230 nm band-pass of the interference O_2 filter, appear as single lines. Since the spectral pattern is symmetrical about the optical axis, the CCD records the lines as rings, corresponding to the K″=3, 5, 7, 9, 11 and 13 transitions.

2.2 OH(6–2) Meinel band

The first three pairs of lines of the Q branch of the OH(6–2) Meinel band appear as pairs of lines with a separation from 0.1 to 0.3 nm, and these pairs are separated from each other by about 0.7 nm. These line pairs, in convolution with the 0.182 nm band-pass of the interference filter, produce two single lines corresponding to the transition K=1 and K=2; the pair of lines corresponding to the transition K=3 appears as two single rings, one of which, $Q_2(3)$, is of an extremely low emission rate.

2.3 Image reduction

An interference filter, centred at λ_0 and having a refractive index μ, transmits the spectral lines of increasing wavelength, λ, at decreasing incidence angles according to the equation:

$$\sin\theta = \mu\sqrt{1-\left(\frac{\lambda_0}{\lambda}\right)^2}. \quad (1)$$

This equation is manipulated to represent $\sin^2\theta = f(\lambda)$. Then, the two parameters μ and λ_0 are found for the rings by a least-squares fitting. The results generally vary from the design values of λ_0 and μ by no more than 0.05 nm and 0.02, respectively.

2.4 Method of rotational temperature and emission rate determination

The method of temperature and emission rate determination is described in detail by Wiens et al. (1991) for the case of the O_2 atmospheric system. Here it is briefly introduced as applied to the temperatures and emission rates, determination from the OH(6–2) Meinel band from one typical OH image.

Figure 1a shows a typical OH image. In order to deduce temperatures and emission rates the airglow spectrum is obtained from the OH image. To obtain the spectrum we need to know the position on the CCD of the ring centre, the wavelength of maximum filter transmission, λ_0, and the effective index of refraction, μ, of the filter. Once the centre is determined the angular radius of each pixel is obtained. The radial variation of the signal of the OH image obtained is shown in Fig. 1b. The radial dimension is changed to wavelength dimension by using Eq. (1). Once the spectral distribution

of the signal is obtained, we use modelled spectra, $mod(\lambda)$, to find the spectrum that best fits the observed spectrum, $exp(\lambda)$. The modelled spectra, $mod(\lambda)$, are obtained by convolving the pure emission spectrum with the finite passband of the OH interference filter. The Gattinger (1984) spectrum for a specific temperature, T, is convolved with the measured passband of the OH interference filter.

The observed spectrum, $exp(\lambda)$, is the result of multiplying this normalized spectrum, $mod(\lambda)$, by some factor, A, and adding a spectrally constant background, B. A least-squares solution of this equation, $exp(\lambda) = A \times mod(\lambda) + B$, for all the radial points from radii 20 to radii 115 provides a estimation of the unknown A and B for each spectrum at the assumed temperature. A library of 150 synthetic spectra, for temperatures between 110° K to 260° K, is used in the least-squares fitting.

The fitting is performed for each spectrum, and the one that yields the minimum fitting error gives its temperature value, T, the emission rate, A, and the continuum background, B. Figure 1c shows the standard deviation of the fit versus temperature and shows that the precision with which the minimum can be specified is ±1° K, or ±2° K at the worst. The fitting of the above OH image is shown in Fig. 1b as a solid line, while the measured values, $exp(\lambda)$, appear as points.

The accuracy involves systematic error, which includes the transition probabilities, errors in the flat field determination, and any possible biases in the fitting of the synthetic spectrum. These matters are currently being investigated in order to make a quantitative estimation of these errors (see Sargoytchev et al., 2004). Sargoytchev et al. (2004) also study the problems associated with the fitting of the lines of the Q branch of the OH(6–2) band. Some of these difficulties are discussed in the next section.

3 Observations

SATI was installed at Sierra Nevada Observatory (37.06° N, 3.38° W), Granada, Spain, at 2900 m height. It has been working continuously since October 1998. Table 1 shows the monthly averaged values presented in this work. The months, with the total number of days, N_d, and hours, N_h, of coverage of each month, the average day of the observations, $\overline{day}$, with 9 October 1998 as the first day of observations. There is a short day of data during August 1998 that has also been included.

Table 1 lists the average rotational temperature and emission rate deduced from both the OH(6–2) Meinel band and the O_2(0–1) atmospheric band for each month. The data analyzed in this work are those corresponding to good observing conditions, days of poor quality of observing conditions have not been considered.

The OH rotational temperatures deduced from the SATI instrument are obtained from the Q branch of the OH(6–2) band. Pendleton and Taylor (2002), based on recent experimental determinations (French et al., 2000), show that the Einstein coefficients for the Q branch of the OH(6–2) band decrease faster with J than previously published coefficients. They have shown that the OH rotational temperatures and emission rates deduced from the Q branch of this band are affected by errors if these previous values are used.

The values of the OH rotational temperatures and emission rates that we report in this paper were obtained using the earlier $A(Q)$ coefficients, but we have applied the correction

Table 1. Airglow observations

Date	N_d	N_h	$\overline{day}$	T_{OH_c} (K)	I_{OH} (R)	T_{O_2} (K)	I_{O_2} (R)
Aug. 1998	1	2	-62.9	195± 5	470± 50	183± 3	370± 30
Sept. 1998							
Oct. 1998	19	78	14.2	211± 7	880±100	201± 6	620±150
Nov. 1998	19	121	42.9	212± 8	850±120	195± 8	410±130
Dec. 1998	10	78	67.3	206± 9	640±130	195±11	460±260
Jan. 1999							
Feb. 1999	17	80	127.3	209± 8	760±120	193± 7	370±100
Mar. 1999	12	76	158.9	204± 9	640±100	196± 6	410±100
Apr. 1999	10	59	187.9	199± 8	600±180	193± 5	360±100
May 1999	5	29	218.0	195± 8	730±110	193± 5	390± 70
June 1999	5	22	247.0	187± 4	690±100	185± 5	460± 70
July 1999	15	52	279.2	179± 6	640±150	184± 5	380± 80
Aug. 1999	5	17	301.9	195± 5	680±100	175± 7	270± 50
Sept. 1999							
Oct. 1999	5	29	366.0	208± 7	590±130	203± 7	440±120
Nov. 1999	9	77	394.0	216± 7	880±160	210± 9	660±150
Dec. 1999	10	75	425.6	215± 8	800±140	201± 9	520±130
Jan. 2000	2	16	460.5	216± 8	970±180	198±10	350±110
Feb. 2000	17	133	485.0	208± 7	750±130	192± 8	340±140
Mar. 2000	14	102	515.5	209± 8	720±140	199± 8	480±130
Apr. 2000	8	48	542.0	207± 7	750±130	196± 6	400± 90
May 2000							
June 2000							
July 2000	4	13	639.8	194± 4	670± 60	176± 5	370± 40
Aug. 2000	18	92	663.5	203± 6	630±120	191± 6	340± 90
Sept. 2000	10	57	697.2	204± 5	640±120	189± 5	320± 80
Oct. 2000	15	79	723.9	207± 7	670±120	194± 7	470±180
Nov. 2000							
Dec. 2000							
Jan. 2001	3	15	834.3	212±13	860±160	188± 9	300± 80
Feb. 2001							
Mar. 2001	15	95	896.5	203± 5	680±130	188± 6	340± 80
Apr. 2001	10	55	927.5	199± 5	590±200	186± 6	290± 70
May 2001	13	61	955.5	194± 8	720±150	181± 7	350± 90
June 2001	8	31	980.5	193± 9	640±120	176± 6	310± 50
July 2001	5	22	1013.0	181± 4	640±120	170± 5	320± 70
Aug. 2001	5	24	1052.1	193± 4	510± 70	182± 7	210± 50
Sept. 2001	10	74	1076.0	195± 6	570±120	187± 6	320± 60
Oct. 2001	14	77	1105.5	204± 7	670±120	197± 6	430± 90
Nov. 2001							
Dec. 2001	5	16	1156.7	212± 7	1000±160	194± 5	330± 60
Jan. 2002	11	81	1196.1	206± 7	650±140	195±12	360± 70
Feb. 2002	13	95	1223.2	203± 6	560±120	190± 8	300±100
Mar. 2002	8	53	1254.8	202± 8	560±150	192± 7	300± 50
				202±6	690±130	190±7	380±100

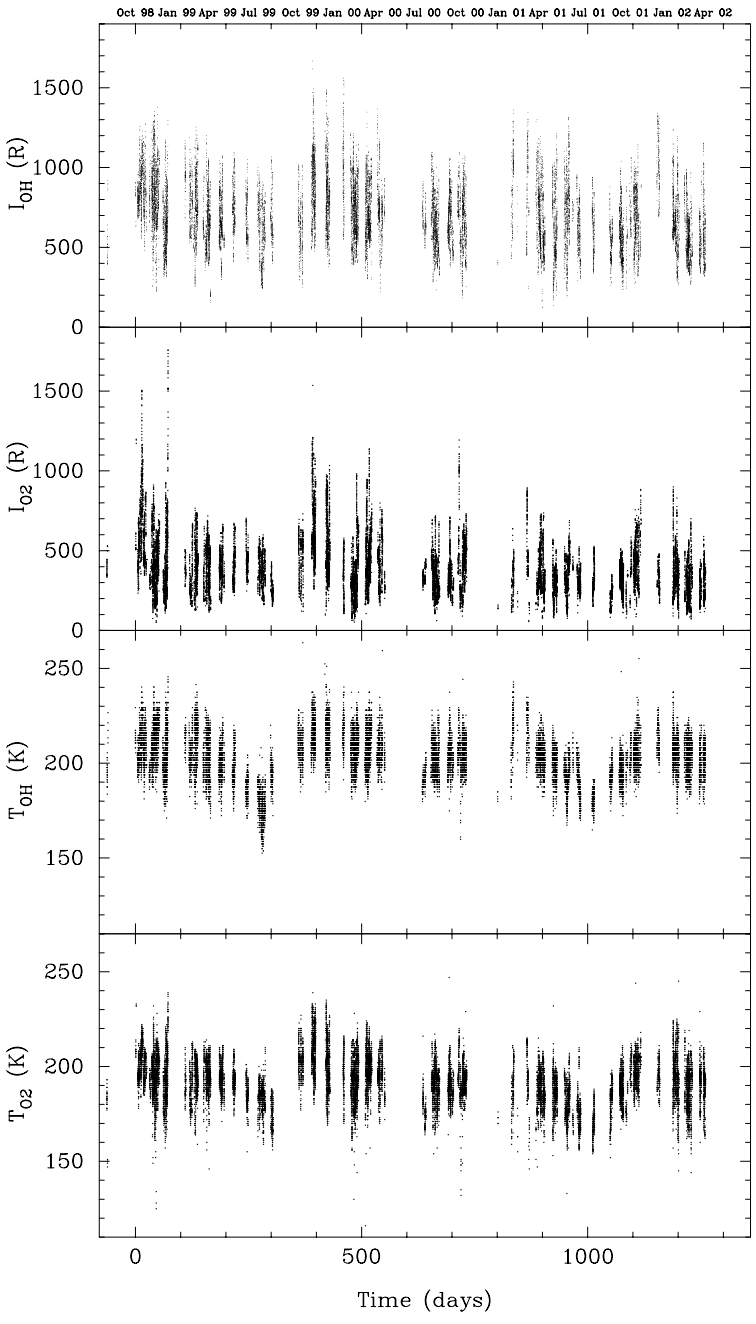

Fig. 2. Rotational temperatures and emission rates.

used by Pendleton and Taylor (2002), before finding a most appropriate correction, to estimate rotational temperatures from the OH(6–2) Meinel band. Thus, the OH rotational temperatures have been corrected (T_{OH_c}) by comparing the temperature obtained from the relative intensities of the $Q_1(1)$ and $Q_1(3)$ Λ-doublets calculated using the theoretical Einstein coefficients with the one obtained using the experimental Einstein coefficients. We will continue to explore this problem with our SATI colleagues at other locations, before making comparisons of the airglow results from other sites. Ultimately, the comparison of our results with those obtained with other similar SATI (Shiokawa et al., 1999) and MORTI (Aushev et al., 2000) instruments, also placed at mid-latitude locations, will be interesting, in order to make a study of the global behaviour of the mesosphere at middle latitudes. In this way, we will contribute to one of the scientific objectives of the Planetary Scale Mesopause Observing System (PSMOS), a project of the Commitee on Solar-Terrestrial Physics (SCOSTEP), and its expected continuation in the Climate And Weather of the Sun-Earth System (CAWSES) project.

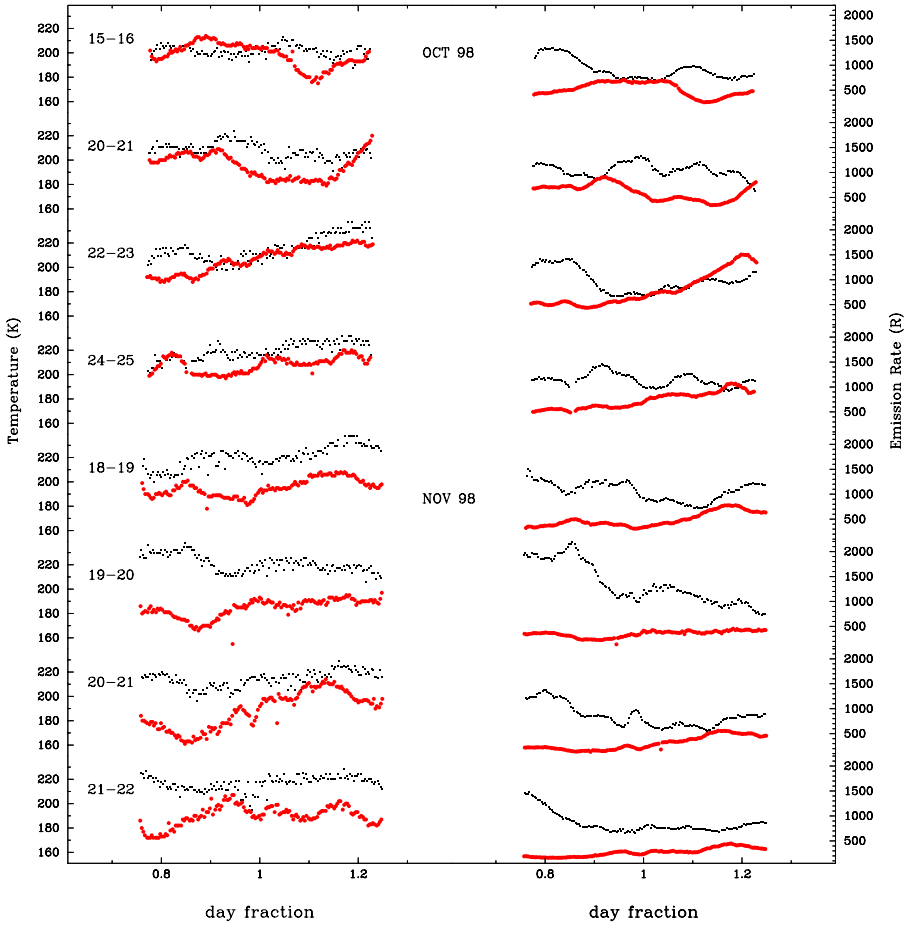

Fig. 3. Rotational temperatures and emission. Dark circles: from the O_2(0–1) atmospheric band. Points: from the OH(6–2) Meinel band.

Figure 2 shows the rotational temperatures and emission rates deduced from both the OH(6–2) Meinel band and from the O_2(0–1) atmospheric band from October 1998 to March 2002. These temperatures and emission rates have been obtained after analysing SATI images as a whole, obtaining then an average of the rotational temperature and emission rate of these airglow bands from the whole sky ring. The vertical scatter of the results indicates the extent of the short-term geophysical variability, but in spite of that there are clear annual and/or semiannual variations.

Figure 3 shows the rotational temperatures and emission rates deduced from the OH(6–2) Meinel band and from the O_2(0–1) atmospheric band during individual nights of October 1998 and November 1998. Looking at Fig. 3 one can see different temporal structures throughout the different nights in temperature and the emission rate, from both OH and O_2 airglow bands. Both rotational temperatures and emission rates vary throughout the night, sometimes in a correlative way, but not always.

The particular features of each day obtained from the whole field of view (see Fig. 3) also appear when the different sectors of the images are analyzed. The analysis of the particular features in the different sectors lets us obtain the characterization of the different waves present during the time of observation and this will be the subject of a future work. Here we characterize the seasonal behaviour in rotational temperature and emission rate from October 1998 to March 2002 taking into account the seasonal tendencies.

4 Results

Mean annual values at different latitudes for T_{OH} and T_{O_2} have been reported (e.g. Shefov, 1971b, 1972; Tepley et al., 1981; Scheer and Reisin, 1990; Takahashi et al., 1995; Greet et al., 1998). At mid latitudes mean annual values of T_{OH} of 204° K at 42.5° N (Niciejewski and Killeen, 1995), and of 190° K at 42° N, with a maximum in winter, 220° K, and a minimum in summer, 160° K, (Choi et al., 1998) have been reported.

Here we find a mean annual value for OH rotational temperature, T_{OH_c}, at 37.06° N of 202±6° K. This mean annual OH rotational temperature, T_{OH_c}, is in the range of values at mid latitudes previously reported and also is in the range of values of WINDII upper mesospheric temperatures (Shepherd et al., 1993), from which a mean annual temperature of 198° K at 87 km height and 35° N is derived (Shepherd et

Table 2. Annual and semiannual variations

	Temperature				Emission Rate			
	OH_c		O_2		OH		O_2	
Mean	202±6		190±7		690±130		380±100	
Period (years)	Amp. (K)	Pha. (rad)	Amp. (K)	Pha. (rad)	Amp. (R)	Pha. (rad)	Amp. (R)	Pha. (rad)
1	14±1	1.7±0.1	9±1	1.7±0.1	90±30	1.6±0.2	50±20	2.3±0.4
1/2	3±1	4.3±0.5	5±1	4.1±0.2	80±20	2.5±0.3	60±20	3.4±0.3

al., 2001, 2004). A mean annual value of 190±7° K from the O_2(0–1) atmospheric band, with maxima temperatures in winter and minima temperatures in summer, is obtained at our latitude.

4.1 Seasonal variations

The seasonal tendencies in the rotational temperature and emission rate are clearly present in Fig. 4, where the monthly averaged night rotational temperature and emission rate deduced from both the OH(6–2) Meinel and the O_2(0–1) atmospheric bands are plotted as a function of the day number. We have only considered nights with at least 1 h of continuous measurements, to obtain a night averaged value, which have then been used to obtain an average value for each month.

To avoid shorter periodicities, we have analyzed the seasonal behaviour of the monthly averaged data. A Fourier analysis of these data clearly shows the presence of a modulation at a time period close to one year, indicating a clear annual variation in the temperatures deduced from both O_2 and OH emissions. This annual variation is also present in both emissions. Other periodic components seem to be present, together with this annual variation. For example, a semiannual variation is present in both emission rates (I_{OH} and I_{O_2}), with a degree of confidence greater than 80%, and also this semiannual component could be present in the temperatures.

The amplitudes that best fit these data for the annual and the semiannual variations are shown in Table 2. These amplitudes have been obtained using a least-squares procedure, to obtain the amplitudes that best fit the data by imposing simultaneously an annual and a semiannual variation. Figure 4 shows the numerical reproductions obtained with these amplitudes.

Figure 4 shows that the annual modulation produces maxima in rotational temperature and emission rate in November–January (winter solstice) and minima in June–August (summer solstice). However, the semiannual variation, produces broader maxima (October–April) and sharper minima (June–August) in temperatures, while for the emissions the opposite is true, sharper maxima (October–December) and broader minima (February–August) in both emission rates (I_{OH} and I_{O_2}) are found. SATI will continue working, and hopefully a large set of data will help us to confirm these seasonal tendencies in both temperatures and emission rates.

The annual component is the most significant in the temperatures deduced from both OH and O_2 emissions. The annual variation in T_{O_2} is almost two times larger than the semiannual variation and the annual variation in T_{OH} is about five times larger than the possible semiannual variation. However, the amplitude of the annual and semiannual variations are of similar magnitude in both emissions.

4.1.1 Temperature

The peak-to-peak amplitude of the temperatures inferred from the OH and O_2 measurements are of about 29° K and 25° K, respectively. T_{OH} variations of 60° K at 42° N (Choi et al., 1998), of 37.5° K at 41° N (She and Lowe, 1998) and of 27° K at 53° N (Mulligan et al., 1995), have been reported. At the mid-latitude Southern Hemisphere T_{OH} variations of about 10° K to 20° K have been reported by Scheer and Reisin (1990) and Hecht et al. (1997). Smaller annual amplitudes have been deduced at low latitudes. In all the cases the annual variations in T_{OH} are strongly present, and a maximum in the winter temperature and a minimum in the summer temperature are reported (e.g. Offermann and Gerndt, 1990; Niciejewski and Killeen, 1995; Bittner et al., 2000), in agreement with the seasonal behaviour found for T_{OH} in this work. Niciejewski and Killeen (1995), from a long-term study of the hydroxyl emission at 42.5° N, found a strong annual behaviour with an amplitude 7 times greater than the amplitude of the semiannual variation also detected. They found a maximum temperature in December (for the annual behaviour) and a maximum at late March and September (for the semiannual variation), with 20° K of amplitude for the annual variation and 3° K of amplitude for the semiannual variation.

We find a strong annual behaviour in T_{OH} with maxima in winter and minima in summer, the maxima are more flattened, while the minima are sharpened (see Fig. 4), in agreement with previous works at mid latitudes. The amplitude for the annual variation of T_{OH_c} found is about five times greater than the amplitude for the semiannual variation (see Table 2).

The seasonal behaviour throughout the year of the T_{O_2}, found here, with maxima in the O_2 rotational temperatures in winter and minima in summer, agrees with that found in

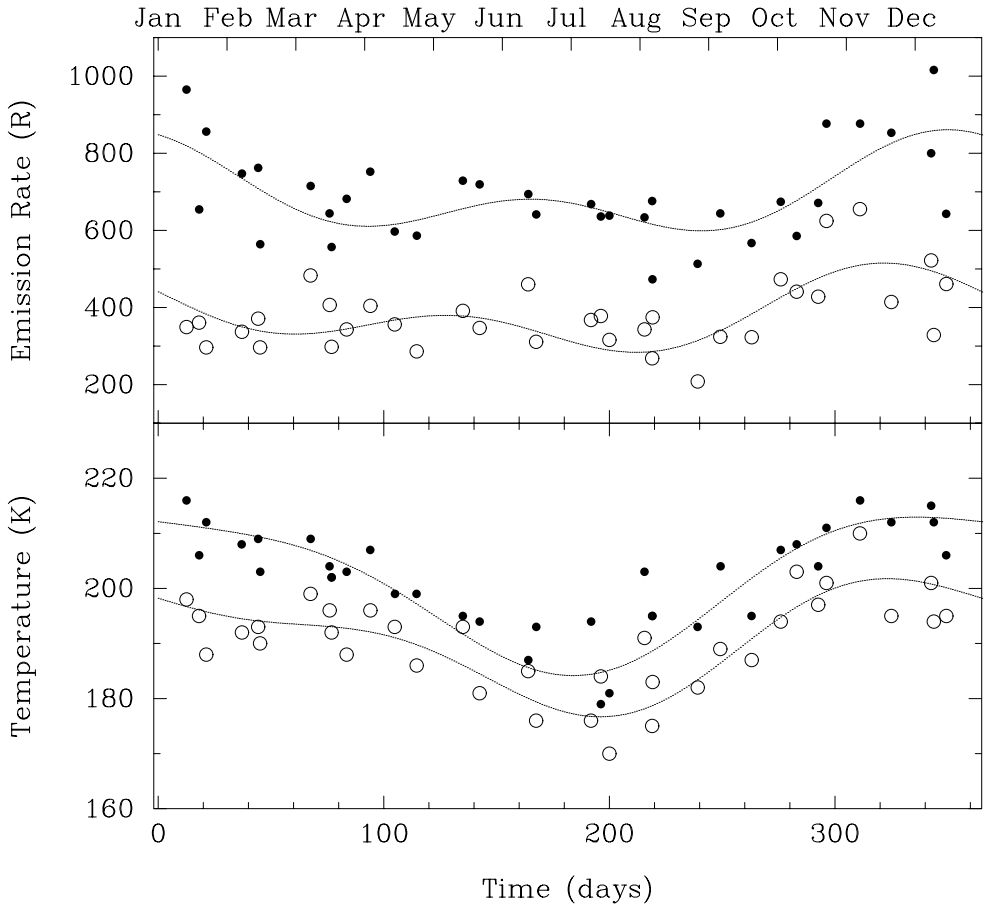

Fig. 4. Average rotational temperatures and emission rates. Open circle: from O_2. Full circle: from OH. Dotted Line: numerical reproduction.

previous measurements at northern latitudes (Shefov, 1971b; Tepley, 1985) but is the opposite of the one found by Scheer and Reisin (1990) at 32°S and by Hecht et al. (1997) at 35° S. Both of them report maximum temperatures in Southern Hemisphere summer and minimum in winter, a behaviour opposite to the one found here.

In the later years, many works have been devoted to the study of the seasonal behaviour of the atmospheric temperature close to the mesopause (She and von Zahn, 1998; She and Lowe, 1998; She et al., 2000). These lidar studies have shown that the mesopause is at an altitude near 100 km in winter and usually also in spring and autumn. At this altitude the annual variation of the temperature is at a minimum. However, the mesopause is found at an altitude near 88 km in summer. At this altitude there exists a maximum annual temperature variation, with the smallest temperatures in summer and larger temperatures in winter. This maximum annual temperature variation decreases from this altitude, where the summer mesopause is found, towards higher altitudes. These studies have also confirmed that the annual temperature variation at this altitude increases with latitude. She et al. (2000), from sodium lidar measurements at (41° N, 105° W) reported maximum annual temperature variations of 41.8° K at 85.5 km (and minimum variation of 9.2° K at 99.5 km), while annual variations of the temperature of about 15° K at 95 km are estimated.

Here we find that the seasonal variation of the OH temperature is about 29° K, while the seasonal variation of the O_2 temperatures is about 25° K. The difference in the seasonal variation of the temperature at about 87 km (OH-layer) and at about 95 km (O_2-layer) is not as great as could be inferred from lidar measurements at (41° N, 105° W). Here, the difference in the seasonal variation of the temperatures inferred from the OH and O_2 airglow layers, can be smoothed in the average process of obtaining the OH and O_2 temperatures from the corresponding airglow layers. Although it might be that the seasonal variation of T_{OH_c} reported in this work could be even greater after finding an improved correction in our OH temperature calculations, it is also true that at 87 km and at 37° N, a little smaller annual variation of temperature than the one at 41° N is expected, and also, the difference in the seasonal variation of the temperatures inferred here, from the OH and O_2 airglow layers could be explained by the approximate 100° longitude difference between the two sites. On the other hand, the similar seasonal behaviour of both O_2 and OH temperatures indicates that the higher or winter

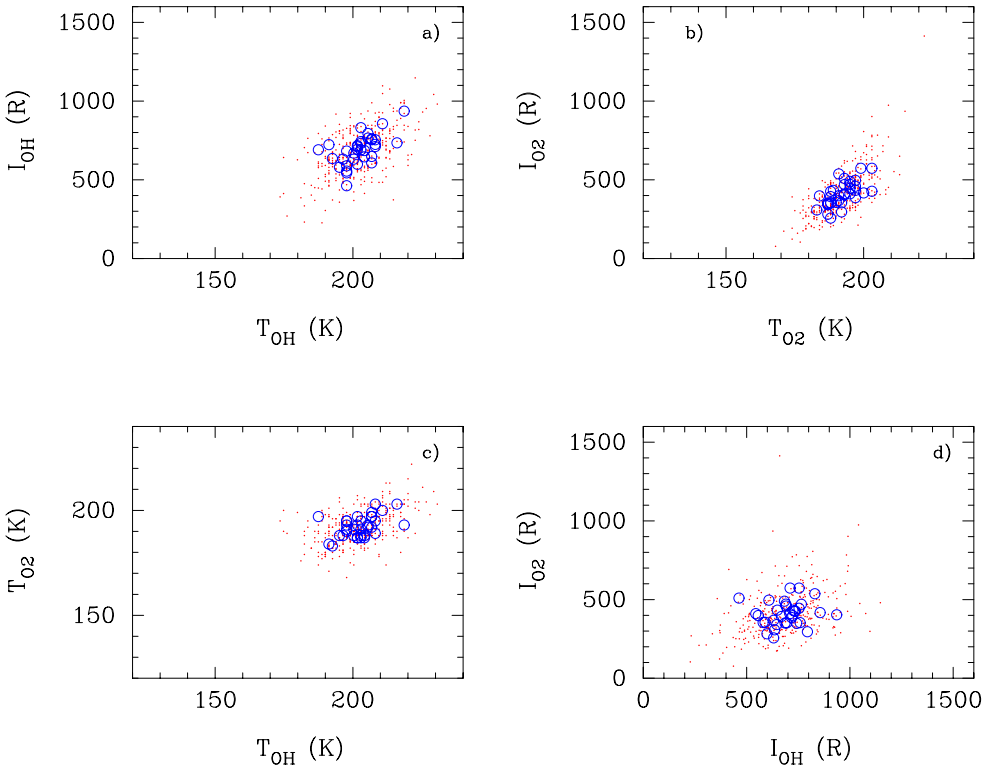

Fig. 5. Relation among emission rates and rotational temperatures. Point: the average value for midnight Circle: the average value for the month. **(a)** I_{OH} versus T_{OH}. **(b)** I_{O_2} versus T_{O_2}. **(c)**T_{O_2} versus T_{OH}. **(d)** I_{O_2} versus I_{OH}.

mesopause is above the O_2 emission layer peak during that period of the year.

The behaviour of the temperature in the altitude region of 80 to 100 km is a very interesting subject. Thus, one of our aims is to obtain a large set of OH and O_2 temperatures with the SATI instrument at our latitude region, to establish the temperature behaviour in this location.

4.1.2 Emission rates

The seasonal behaviour of I_{OH} emission shows different patterns at different latitudes. OH emission measurements, at different latitudes, have shown that there is a semiannual seasonal behaviour for I_{OH} at equatorial latitudes that evolves to an annual behaviour at high latitudes (e.g. Wiens and Weill, 1973; Shefov and Piterskaya, 1984; Takahashi et al., 1995; Melo et al., 1999). Here we obtain an annual behaviour with a semiannual component, that produces a great maximum towards December and a small maximum in June, in agreement with the results obtained by Wiens and Weill (1973) at 44° N latitude.

Many O_2(0–1) airglow observations have shown that the seasonal behaviour of O_2(0–1) emission is also dependent on latitude (e.g. Shefov, 1971b; Misawa and Takeuchi, 1982; Burrage et al., 1994; Yee et al., 1997). These observations have shown that the seasonal variation of the O_2(0–1) emission is predominantly semiannual at low latitudes, evolving to a stronger annual variation at high latitudes. The behaviour found in the O_2(0–1) emission obtained from the SATI instrument follows this pattern. We find an annual variation with maximum in winter (November–December), but together an almost equal powerful semiannual component that produces smaller maxima towards May.

4.2 Relations between OH and O_2 emission rates and rotational temperatures

Figure 5 shows scatter plots of the rotational temperatures and emission rates after the seasonal dependences have been removed from the data, for the annual and semiannual component listed in Table 2. Figure 5a shows I_{OH} as function of T_{OH}; as can be seen the general tendency is that I_{OH} increases with T_{OH} (the correlation index for a possible linear relation between T_{OH} and I_{OH} is of about of 45%–55%).

However, a clearer dependence seems to exist between I_{O_2} and T_{O_2} (see Fig. 5b), with a correlation coefficient of about 65%–70% for a linear relation. The dependency of I_{OH} with T_{OH} is not as clear; it could be an indication that the OH(6–2) emission is more affected by other atmospheric parameters, while the I_{O_2} emission has a stronger dependence on the temperature. After removing the seasonal dependences of T_{O_2} and T_{OH}, there still remains a certain relation between both temperatures. A correlation coefficient of 40%–45% for a linear relation between both rotational temperatures is found (see Fig. 5c). There is not any clear relation between I_{O_2} and I_{OH} (see Fig. 5d).

5 Conclusions

The results for temperatures and emission rates deduced from the OH(6–2) Meinel and O_2(0–1) atmospheric bands after more than three years of SATI operation have been presented. Seasonal variations in emission rates and rotational temperatures have been obtained for a latitude of 37.06° N.

A clear annual variation is found in temperatures and an annual variation, together with a semiannual variation of similar magnitude, is found in the emission rates. The range of variability detected in both emissions and temperatures is in agreement with the ones reported at mid latitudes in previous works. The mean temperature of T_{OH_c} is a little greater than that obtained for T_{O_2}, and both show a similar seasonal behaviour. The magnitude of the seasonal variation of the temperature at about 87 km (T_{OH}) is a little greater than that at about 95 km (T_{O_2}). Sodium lidar measurements at mid latitudes have shown a larger difference in the magnitude of the seasonal variation of the temperature at 87 km and 95 km, than from our data. Although it might be that the annual amplitude variation of T_{OH} could be larger after finding a better method for the OH temperature calculations, the seasonal variation of the temperature presented here is recorded at (37° N, 3° W) and the one reported from mid latitude lidar measurements at (41° N, 105° W), so the differences could be the result of the different location of the two sites.

A stronger dependence seems to exist between T_{O_2} and I_{O_2} than the dependence between I_{OH} and T_{OH}. This could indicate that OH emission is more affected by other influences, while O_2(0–1) atmospheric emission is more temperature dependent.

6 Future work

The necessity of long-term programs of observing airglow emissions from low, middle and high latitudes in a simultaneous coverage is pointed out in order to know the global seasonal behaviour of different atmospheric parameters, including temperature and chemical constituents. In this sense, one of the objectives of the PSMOS project was to cover low, mid and high latitudes, to study the long-term behaviour of the upper atmosphere. This objective will be continued in the CAWSES project. Data are needed to understand the chemical and dynamical processes that are producing the seasonal tendencies observed at different latitudes. In this sense, data from SATI of emission rates and rotational temperatures of O_2 and OH emissions will be added to other sets of data obtained at similar latitudes (Almaty, London, Shigaraki), together with other sets of data coming from lower and higher latitudes, with the object of making a global study to understand the processes that are producing the variabilities detected in the upper atmosphere. We still have to find a way to more precisely deduce OH rotational temperatures from the Q branch of the (6–2) band, in order to make compatible the results obtained with this SATI instrument and the ones obtained from other instruments.

Acknowledgement. This research was partially supported by the Dirección General de Investigación (DGI) under projects AYA2000-1559 and ESP2002-04256, the Comisión Interministerial de Ciencia y Tecnología under project REN 2001-3249, the Junta de Andalucía and the NATO under a Collaborative Linkage Grant. We very gratefully acknowledge the staff of Sierra Nevada Observatory for their help and assistance with SATI instrument. We wish to thank the referees, R. P. Lowe and another anonymous referee, for their useful comments and suggestions.

Topical Editor U.-P. Hoppe thanks R. P. Lowe and another referee for their help in evaluating this paper.

References

Aushev, V. M., Pogoreltsev, A. I., Vodyannikov, V. V., Wiens, R. H., and Shepherd, G. G.: Results of the Airglow and Temperature Observations by MORTI at the Almaty Site (43.05 N, 76.97 E), Phys. Chem. Earth 25, 409–415, 2000.

Baker, D. J. and Stair Jr., A. T.: Rocket measurements of the altitude distribution of hydroxyl airglow, Phys. Scripta, 37, 611–622, 1988.

Bittner, M., Offermann, D., and Graef, H. H.: Mesopause temperature variability above a midlatitude station in Europe, J. Geophys. Res., 105, 2045–2058, 2000.

Burrage, M. D., Arvin, N., Skinner, W. R., and Hays, P. B.: Observations of the O_2 atmospheric band nightglow by the High Resolution Doppler Imager, J. Geophys. Res., 99, 15 017–15 023, 1994.

Choi, G. H., Monson, I. K., Wickwar, V. B., and Rees, D.: Seasonal variations of temperature near the mesopause from Fabry-Perot interferometer observations of OH Meinel emissions, Adv. Space Res., 21, 843–846, 1998.

French, W. J. R., Burns, G. B., Finlayson, K., Greet, P. A., Lowe, R. P., and Williams, P. F. B.: Hydroxyl (6–2) airglow emission intensity ratios for rotational temperature determination, Ann. Geophysicae, 18, 1293–1303, 2000.

Gattinger, R. L.: Synthetic spectrum of OH Meinel bands, Herzberg Institute of Astrophysics Software, Ottawa, 1984.

Greer, R. G. H., Murtagh, D. P., McDade, I. C., Dickinson, P. H. G., Thomas, L., Jenkins, D. B., Stegman, J., Llewellyn, E. J., Witt, G., Mackinnon, D. J., and Williams, E. R.: Eton 1: A date base pertinent to the study of energy transfer in the oxygen nightglow, Planet. Space Sci., 34, 771–788, 1986.

Greet, P. A., French, W. J. R., Burns, G. B., Williams, P. F. B., Lowe, R. P., and Finlayson, K.: OH(6-2) spectra and rotational temperature measurements at Davis, Antarctica Ann. Geophysicae, 16, 77–89, 1998.

Hecht, J. H., Walterscheid, R. L., Woithe, J., Campbell, L., Vicent, R. A., and Reid, I. M.: Trends of airglow imager observations near Adelaide, Australia, Geophys. Res. Lett., 24, 587–590, 1997.

Meinel, A. B.: OH emission bands in the spectrum of the night sky. I., Astrophys. J., 111, 555–564 , 1950a.

Meinel, A. B.: O_2 emission bands in the infrared spectrum of the night sky, Astrophys. J., 112, 464–468 , 1950b.

Melo, S. M. L., Lowe, R. P., and Takahashi, H.: The nocturnal behavior of the hydroxyl airglow at equatorial and low latitudes as observed by WINDII: Comparison with ground-based measurements, J. Geophys. Res., 104, 24 657–24 665, 1999.

Misawa, K. and Takeuchi, I.: Ground observations of the O_2(0–1) atmospheric band at 8645 Å and the [OI] 5577 Å line, J. Geo-

phys. Res., 82, 2410–2412, 1977.

Misawa, K. and Takeuchi, I.: Nightglow intensity variations in the O_2(0–1) atmospheric band, the NaD lines, the OH(6–2) band, the yellow-green continuum at 5750 Å and the oxygen green line, Ann. Geophysicae, 38, 781–788, 1982.

Mulligan, F. J., Horgan, D. F., Galligan, J. G., and Griffin, E. M.: Mesopause temperatures and integrated band brightness calculated from airglow OH emissions recorded at Maynooth (53.2° N, 6.4° W) during 1993, J. Atmos. Terr. Phys., 57, 1623–1637, 1995.

Niciejewski, R. J. and Killeen, T. L.: Annual and semi-annual temperature oscillations in the upper mesosphere, Geophys. Res. Lett., 22, 3243–3246, 1995.

Offermann, D. and Gerndt, R.: Upper-mesosphere temperatures from OH emissions, Adv. Space Res., 10, 217–221, 1990.

Pendleton Jr., W. R. and Taylor, M. J.: The impact of L-uncoupling on Einstein coefficients for the OH Meinel (6,2) band: implications for Q-branch rotational temperatures, J. Atmos. Solar-Terr. Phys., 64, 971–983, 2002.

Sargoytchev, S., Brown, S., Solheim, B. H., Cho, Y.-M., Shepherd, G. G, and López-González, M. J.: Spectral airglow temperature imager (SATI) – a ground based instrument for temperature monitoring of the mesosphere region, accepted, Applied Optics, 2004.

Scheer, J. and Reisin, E. R.: Rotational temperatures for OH and O_2 airglow bands measured simultaneously from El Leoncito (31°48'S), J. Atmos. Terr. Phys., 52, 47–57, 1990.

She, C. Y. and Lowe, R. P.: Seasonal temperature variations in the mesopause region at mid-latitude: comparison of lidar and hydroxyl rotational temperatures using WINDII/UARS OH Height profiles, J. Atmos. Solar-Terr. Phys., 60, 1573–1583, 1998.

She, C. Y. and von Zahn, U.: Concept of a two-level mesopause: Support through new lidar observations, J. Geophys. Res., 103, 5855–5864, 1998.

She, C. Y., Chen, S., Hu, Z., Sherman, J., Vance, J. D., Vasoli, V., White, M. A., Yu, J., and Krueger, D. A.: Eight-year climatology of nocturnal temperature and sodium density in the mesopause region (80 to 105 km) over Fort Collins, CO (41° N, 105° W) Geophys. Res. Lett., 27, 3289–3292, 2000.

Shefov, N. N.: Hydroxyl emission of the upper atmosphere – I. Behaviour during a solar cycle, seasons and geomagnetic disturbances, Planet. Space Sci., 17, 797–813, 1969.

Shefov, N. N.: Hydroxyl emission of the upper atmosphere – III. Diurnal variations, Planet. Space Sci., 19, 129–136, 1971a.

Shefov, N. N.: Hydroxyl emission of the upper atmosphere – IV. Correlation with the molecular oxygen emission, Planet. Space Sci., 19, 795–796, 1971b.

Shefov, N. N.: Hydroxyl emission, Annales de Geophysique, 28, 137–143, 1972.

Shefov, N. N. and Piterskaya, N. A.: Aurorae and Airglow, U. S. S. R. Acad. Sci., 31, 23, 1984.

Shepherd, G. G., Thuillier, G., Gault, W. A., Solheim, B. H., Hersom, C., Alunni, J. M., Brun, J.-F., Brune, S., Charlot, P., Cogger, L. L., Desaulniers, D.-L., Evans, W. F. J., Gattinger, R. L., Girod, F., Harvie, D., Hum, R. H., Kendall, D. J. W., Llewellyn, E. J., Lowe, R. P., Ohrt, J., Pasternak, F., Peillet, O., Powell, I., Rochon, Y., Ward, W. E., Wiens, R. H.,and Wimperis, J.: WINDII, the wind imaging interferometer on the Upper Atmosphere Research Satellite, J. Geophys. Res., 98, 10 725–10 750, 1993.

Shepherd, M. G., Reid, B., Zhang, S. P., Solheim, B. H., Shepherd, G. G. Wickwar, V. B., and Herron, J. P.: Retrival and validation of mesospheric temperatures from wind imaging interferometer observations, J. Geophys. Res., 106, 24 813–24 829, 2001.

Shepherd, M. G., Rochon, Y. I., Offermann, D., Donner, M., and Espy P. J.: Longitudinal variability of mesospheric temperatures during equinox at middle and high latitudes, accepted, J. Atmos. Solar-Terr. Phys., 2004.

Shiokawa, K., Katoh, Y., Satoh, M., Ejiri, M. K., Ogawa, T., Nakamura, T., Tsuda, T., and Wiens, R. H.: Development of Optical Mesosphere Thermosphere Imagers (OMTI), Earth, Planets and Space, 51, 887–896, 1999.

Takahashi, H., Sahai, Y., Clemesha, B. R., Batista, P. P., and Teixeira, N. R.: Diurnal and seasonal variations of the OH (8,3) airglow band and its correlation with OI 5577 Å, Planet. Space Sci., 25, 541–547, 1977.

Takahashi, H., Sahai, Y., and Batista, P. P.: Airglow $O_2(^1\Sigma)$ atmospheric band at 8645 Åand the rotational temperature observed at 23°S, Planet. Space Sci., 34, 301–306, 1986.

Takahashi, H., Clemesha, B. R., and Batista, P. P.: Predominant semi-annual oscillation of the upper mesospheric airglow intensities and temperatures in the equatorial region, J. Atmos. Terr. Phys., 57, 407–414, 1995.

Tepley, C. A., Burnside, R. G., and Meriwether Jr., J. W.: Horizontal thermal structure of the mesosphere from observations of OH(8-3) band emissions, Planet. Space Sci., 29, 1241–1249, 1981.

Tepley, C. A.: A nonlinear least-squares approach to the analysis of O_2(0–1) atmospheric band emissions, Ann. Geophysicae, 3, 177–180, 1985.

Wiens, R. H. and Weill, G.: Diurnal, annual and solar cycle variations of hydroxyl and sodium nightglow intensities in the Europe-Africa sector, Planet. Space Sci., 21, 1011–1027, 1973.

Wiens, R.H., Moise, A., Brown, S., Sargoytchev, S., Peterson, R. N., Shepherd, G. G., López-González, M. J., López-Moreno, J. J., and Rodrigo, R.: SATI: A Spectral Airglow Temperature Imager, Adv. Space Res., 19, 677–680, 1997.

Wiens, R. H., Zhang, S. P., Peterson, R. N., and Shepherd, G. G.: MORTI: A Mesopause Oxygen Rotational Temperature Imager, Planet. Space Sci., 39, 1363–1375, 1991.

Witt, G., Stegman, J., Solheim, B. H., and Llewellyn, E. J.: A measurement of the $O_2(b^1\Sigma_g^+ - X^3\Sigma_g^-)$ atmospheric band and the OI(^{1}S) green line in the nightglow, Planet. Space Sci., 27, 341–350, 1979.

Witt, G., Stegman, J., Murtagh, D. P., McDade, I. C., Greer, R. G. H., Dickinson, P. H. G., and Jenkins, D. B.: Collisional energy transfer and the excitation of $O_2(b^1\Sigma_g^+)$ in the atmosphere, J. Photochem., 25, 365–378, 1984.

Yee, J. H., Crowley, G., Roble, R. G., Skinner, W. R., Burrage, M. D., and Hays, P. B.: Global simulations and observations of $O(^1S)$, $O_2(^1\Sigma)$ and OH mesospheric nightglow emissions, J. Geophys. Res., 102, 19 949–19 968, 1997.

Zhang, S.P., Peterson, R. N., Wiens, R. H.,and Shepherd, G. G.: Gravity waves from O_2 nightglow during the AIDA'89 campaign I: emission rate/ temperature observations, J. Atmos. Terr. Phys., 55, 355–375, 1993.